ORIGINAL ARTICLE

Biosynthesis of gold nanoparticles by *Bacillus marisflavi* and its potential in catalytic dye degradation

Nilofar Yakub Nadaf, Shivangi Shivraj Kanase [*]

P.G. Department of Microbiology, Yashvantrao Chavan Institute of Science, Satara, Maharashtra 415 001, India

Abstract   The development of an eco-friendly protocol for the synthesis of nanomaterial is an important aspect of research in nanotechnology. This is the first report describing a greener approach for the extracellular synthesis of gold nanoparticles using *Bacillus marisflavi* YCIS MN 5. The addition of gold chloride solution into a cell-free extract (CFE) of *B. marisflavi* resulted in the synthesis of gold nanoparticles at room temperature within 96 h. The biosynthesized gold nanoparticles were thoroughly characterized by physicochemical characterization techniques. The synthesized nanoparticles were found to be crystalline and spherical with an average size in the range of ∼14 nm. The CFE acted both as reducing and stabilizing agents; hence, no additional capping and the stabilizing agents were needed. These gold nanoparticles were assessed for catalytic reduction of Congo red and methylene blue. It was established that the reduction reaction follows pseudo-first order kinetics with a reaction rate constant of 0.2192 and 0.2484 min^{-1} for Congo red and methylene blue, respectively. Thus, the synthesized gold nanoparticles were found to show outstanding catalytic activity in the degradation of Congo red and methylene blue. The degraded products were identified by Gas chromatography-mass spectroscopy (GC-MS) after the degradation of Congo red and methylene blue. These results suggest *B. marisflavi* mediated synthesized gold nanoparticles as a promising nano-catalyst in the degradation of Congo red and methylene blue.

1. Introduction

Metal nanoparticles have occupied the center of scientific attention due to their fascinating chemical, optical and electronic properties. Among them, gold nanoparticles have drawn remarkable research interest in the recent years because of their higher stability and size related electronic, optical and spectroscopic properties (Njoki et al., 2007). They have been widely applied in various fields (Saha et al., 2012; Versiani et al., 2016). However, the synthesis of gold nanoparticles possessing desired properties is an important task. More commonly gold nanoparticles are synthesized using bottom-up strategies such as

[*] Corresponding author.
  E-mail addresses: nadaf_mcft@rediffmail.com (N.Y. Nadaf), srkanase@rediffmail.com (S.S. Kanase).
Peer review under responsibility of King Saud University.

chemical reduction methods, using the reducing, protective and stabilizing agents. These agents are mostly toxic, flammable (Rai et al., 2011), may adsorb on the nanoparticles surface and also have adverse effects in biological applications (Philip, 2010). Due to these limitations, greener approach for the synthesis of nanoparticles is preferred. Such synthesis of nanoparticles using biological approaches is facile, eco-friendly and provides an easy way to achieve increasing global need of clean, non-toxic and biocompatible nanoparticles.

Biological synthesis of nanoparticles using microbes has been of special interest to the researchers because of easy handling procedures, eco-friendly disposal and much easier downstream processing (Velusamy et al., 2016). Among different microbes, bacteria possess the innate ability to synthesize metal nanoparticles by reducing the respective metal (Srivastava and Constanti, 2012). Recently, eco-friendly synthesis of silver, selenium, titanium dioxide, and gold (metal) nanoparticles using various bacterial strains such as, *Bacillus* sp., *B. amyloliquefaciens*, *B. clausii*, and *Azoarcus* sp. has been reported (Elbeshehy et al., 2015; Fernández-Llamosas et al., 2016; Khan and Fulekar, 2016; Singh et al., 2016; Zhang et al., 2016).

Nowadays, various organic dyes are widely used in textile, food, cosmetics, leather, paper and plastic industries for esthetic purposes. Most of them are potentially hazardous and poses a great threat to the environment. Congo red is the secondary diazo dye widely used in textile industry. This dye is water soluble, highly stable and resistant to biodegradation. Its bright red color affects the esthetic beauty of aquatic environment as well. Methylene blue is another heterocyclic aromatic azo dye increasingly used in paint production and textile industries. It is a monoamine oxidase inhibitor (Cohen and Smetzer, 2016), and upon intravenous infusion it causes severe serotonin toxicity (Gillman, 2006).

The treatment and removal of organic dyes from textile effluent is one of the challenging tasks faced by the environmentalists and industries. Various physicochemical methods such as coagulation, adsorption on activated carbon, ultrafiltration, and reverse osmosis are already in practice. However, these are ineffective and lead to the generation of new compounds which require further treatments. In the recent years, modern technologies involving the use of nanocatalyst in the removal of dyes and other organic pollutants from the environment are gaining considerable attention. The treatment of dyes in the presence of biocompatible, eco-friendly nanocatalyst is the straightforward route which does not involve the use of organic solvents. In this context, efforts were made to search for an eco-friendly source for the synthesis of gold nanoparticles and to assess their role as a catalyst in degradation of organic pollutant. Here we report, for the first time, a facile and bacteriogenic route to synthesize gold nanoparticles using *Bacillus marisflavi* YCIS MN 5 and proposed their potential catalytic activity in the degradation of Congo red and methylene blue in the presence of sodium borohydride (NaBH$_4$).

2. Materials and methods

2.1. Chemicals and media

For this study, HAuCl$_4$ (purity 99%), nutrient agar, and broth were procured from Himedia laboratories Pvt., Ltd., India. Congo red, methylene blue NaBH$_4$, diethyl ether, CaCl$_2$ and methanol were obtained from Merck Pvt., Ltd., India. All chemicals were of analytical reagent grade.

2.2. Biosynthesis of gold nanoparticles

The bacterial strain, *Bacillus marisflavi* YCIS MN 5 (hereafter *B. marisflavi*) was isolated from estuarine water at Dabhol, India. Molecular identification of the bacterial isolate was carried out by 16S rRNA sequencing at Microbial Culture Collection (MCC), Pune, India (refer Nadaf and Kanase, 2015). The 16S rRNA sequence was deposited in the NCBI Gene Bankit nucleotide sequence database (accession number KP163987; Nadaf and Kanase, 2015).

The pure culture of *B. marisflavi* was inoculated into the sterile nutrient broth and incubated at room temperature for 24 h at 120 rpm. Further, the biomass was collected, washed, suspended in sterile distilled water (DW) and agitated (120 rpm) at room temperature for 24 h. The supernatant (cell-free extract) collected after centrifugation was used for the synthesis of nanoparticles. The equal volume of 1 mM HAuCl$_4$ solution was mixed with cell-free extract (CFE) and agitated (at 120 rpm) in the dark at room temperature. Simultaneously, 1 mM HAuCl$_4$ solution was maintained as a control under similar conditions. To probe the role of biomolecules (acting as reducing agents) present in the CFE, one set of experiments was also performed where heat treated CFE was challenged with 1 mM HAuCl$_4$ solution. The formation of gold nanoparticles was routinely monitored by visual inspection as well as recording the UV-Visible spectra of the reaction mixture.

2.3. Characterization of the gold nanoparticles

The excitation spectrum of the biosynthesized gold nanoparticle was measured at regular time intervals by UV-Visible spectrophotometer (Systronics Au-270 I) in the wavelength range of 350–800 nm. The crystallographic information of gold nanoparticles was obtained by X-ray diffraction (XRD) analysis on Bruker D8 ADVANCE diffractometer with CuKα (1.5406 Å) radiation. The XRD was operated at 40 kV and 40 mA at a 2 theta range of 20–80°. Prior to XRD analysis, the gold colloidal solution was centrifuged at 12,000 rpm for 20 min. The pellet was repeatedly washed and suspended in DW. A dense film of this solution was deposited on a glass slide by drop-casting and air dried to carry out the XRD analysis. The information about morphology and size of the gold nanoparticles was obtained by field emission scanning electron microscopy (FESEM, FEI Model-Nova NanoSEM 450). The transmission electron microscopic (TEM) imaging of gold nanoparticles deposited on the carbon-coated copper grid was carried out under FEI Tecnai G2 U-Twin TEM at 200 kV. Dynamic light scattering (DLS, Nicomp 388 ZLS, PSS Nicomp Particle sizing systems, Inc., USA) technique was used to determine the particle size. Fourier transform infrared (FTIR, Shimadzu FTIR 8400) spectroscopy was performed over the range of 400–4000 cm^{-1} to investigate the involvement of biomolecules in gold nanoparticles synthesis.

2.4. Catalytic activity of biosynthesized gold nanoparticles in the degradation of Congo red and methylene blue

For catalytic decomposition of Congo red, 1 ml of freshly prepared NaBH$_4$ (0.150 M) solution was mixed with 1 ml of Congo red (1 mM), the total volume adjusted to 3 ml with DW. 500 μl of gold nanoparticles solution (50 μg/ml) was added to the above solution and gently mixed (Mata et al., 2015). The reaction mixture without gold nanoparticles was kept as control. UV-Visible absorbance spectra were recorded in the range of 300–700 nm at 5 min time interval in UV-vis spectrophotometer. For methylene blue catalytic degradation,

5.77 ml of DW was added to 30 μl of 0.01 M methylene blue and 200 μl of 0.1 M NaBH$_4$. Further 200 μl gold nanoparticles (50 μg/ml) solution was added to this reaction mixture. The content was mixed and observed for color change (Narayanan and Park, 2014). The time-dependent reduction of dyes was quantitatively measured by recording UV-visible spectra in the range of 500–800 nm at a 1 min time interval. The control without gold nanoparticles was also monitored for color change.

2.5. Gas chromatography mass spectroscopy (GC-MS) analysis of degraded dyes

To study the formation of metabolites upon catalytic degradation of Congo red and methylene blue, the decolorized solution of both dyes was centrifuged to remove catalyst particles. The supernatant obtained was extracted thrice with an equal volume of diethyl ether using a separating funnel. The solvent phase was collected, dried over CaCl$_2$, and dissolved in HPLC grade methanol. The GC-MS (Shimadzu GCMS-TQ 8030; Rtx 5M S) analysis was conducted in temperature programming mode with ionization voltage of 70 eV. The initial column temperature was 80 °C for 2 min then increased linearly at 10 °C min^{-1} to 280 °C and held for 7 min. The temperature of the injection port was 280 °C and the GC-MS interface was maintained at 290 °C. Helium was used as carrier gas with a flow rate of 1.0 ml min^{-1}.

3. Results and discussion

3.1. Biosynthesis of gold nanoparticles

In this study, the previously isolated bacterial strain, *B. maris-flavi* (Nadaf and Kanase, 2015) was used further to investigate its ability to synthesize gold nanoparticles. The extracellular synthesis of gold nanoparticles using CFE was verified by the gradual color change from pale yellow to bluish purple. The color developed within 24 h, and the intensity of color increased up to 96 h. The blue-violet coloration (Supplementary Fig. 1b) is due to the surface plasmon resonance (SPR) which indicates the formation of gold nanoparticles. The control tube containing heat-treated CFE with 1 mM HAuCl$_4$ (Supplementary Fig. 1a) and only 1 mM HAuCl$_4$ solution (data not shown) remained pale yellow. The control tube containing heat-treated CFE with 1 mM HAuCl$_4$ remained pale yellow most probably due to the denaturation of the biomolecules. This suggests the role of biomolecules specifically proteins in the synthesis of gold nanoparticles.

3.2. Characterization of the gold nanoparticles

UV-visible spectroscopy is a useful technique to study the kinetics of the formation of gold nanoparticles. The results showed the absorption peak at 560 nm, the intensity of which increased gradually with time. The complete reduction of Au ions took place in 96 h (Fig. 1). The occurrence of an absorption peak in the range 500–600 nm indicates the formation of the gold nanoparticles which may be due to excitation of SPR (Baharara et al., 2016). Previous studies showed the appearance of the resonance peak of gold nanoparticles
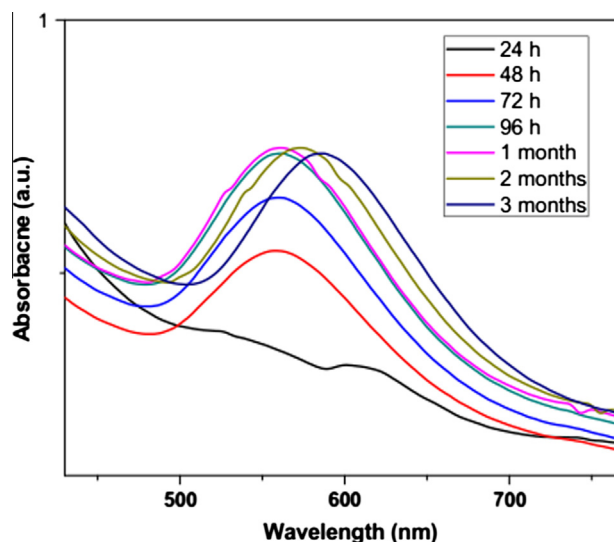

Figure 1   The UV-visible spectrum of a colloidal solution of gold nanoparticles synthesized using *B. marisflavi* showing strong SPR peak at 560 nm.
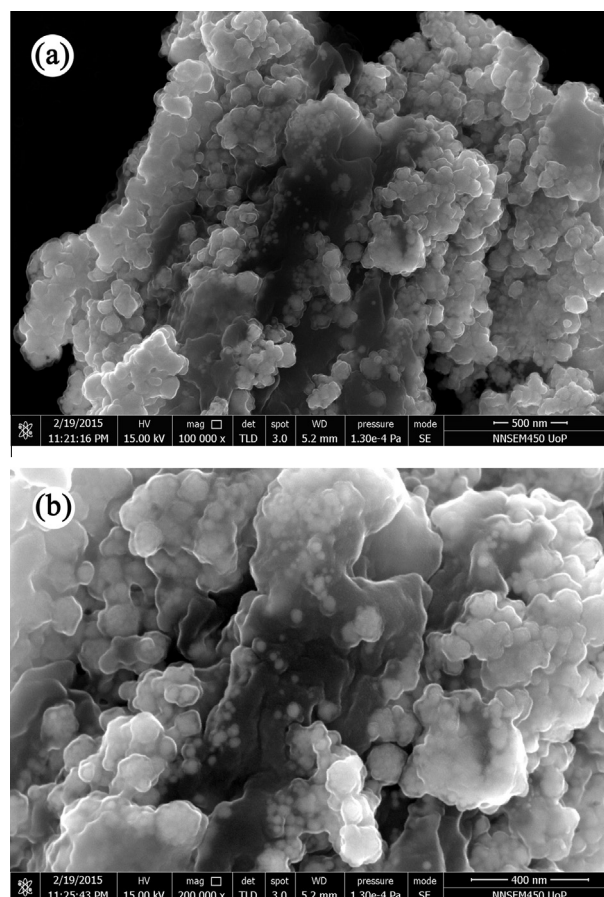

Figure 2   FESEM images of gold nanoparticles (a) at a magnification of 100,000× and (b) at a magnification of 200,000×.

around this region, but the exact position may vary due to certain factors such as size and shape of the nanostructures (Hu et al., 2006). The stability of gold nanoparticles was also
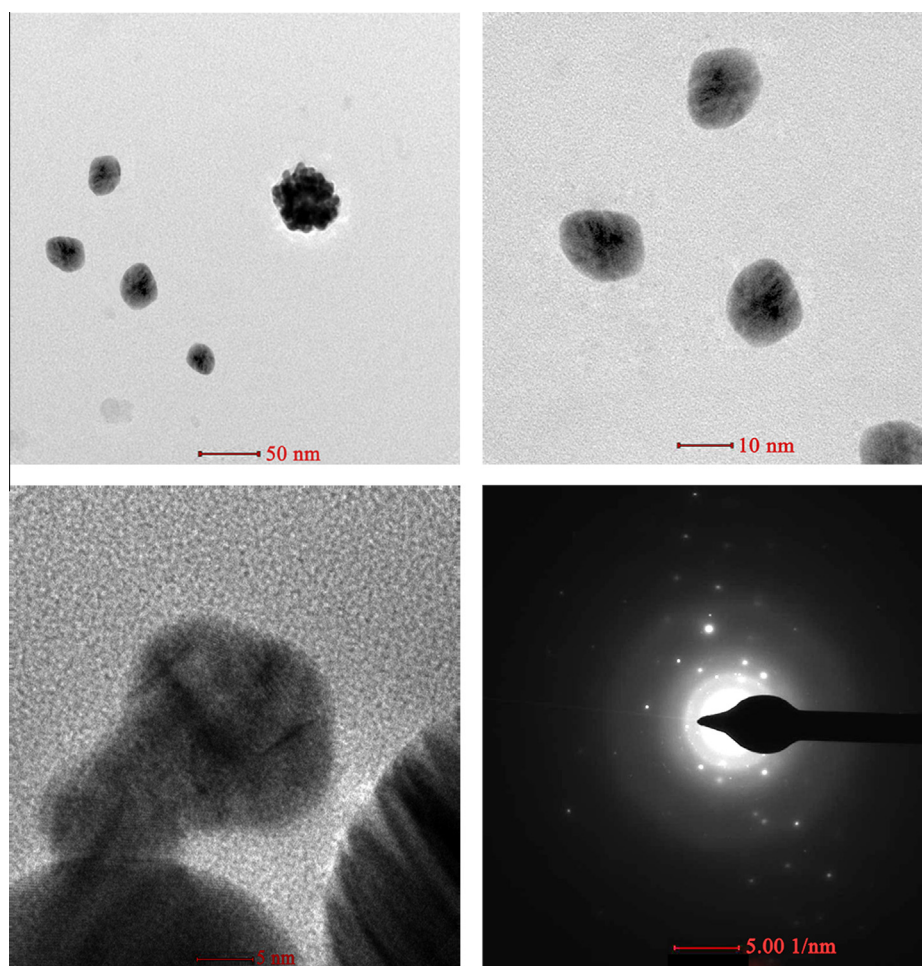
Figure 3   TEM images of biosynthesized gold nanoparticles (a–c) under different magnifications; (d) corresponding SAED pattern of biosynthesized gold nanoparticles.
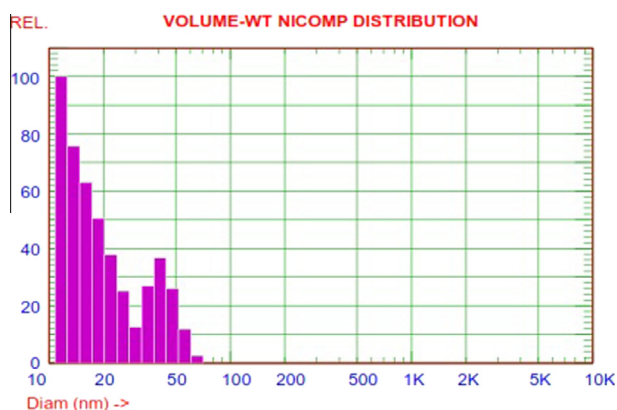

Figure 4   Hydrodynamic particle size measurement using DLS (volume weighted) technique.

studied by recording the UV-Visible spectra over a longer period of time. It was observed that the synthesized gold nanoparticles were stable for one month without shift in peak. However after one month, the red shift in peak position was observed (Fig. 1). To gain further insight into the formation and crystallinity of synthesized gold nanoparticles, the XRD

analysis was performed. The four prominent Bragg's peaks appeared over the range of 2 Theta values from 20° to 80°. The pattern showed diffraction peaks at 38.20°, 44.28°, 64.66°, 77.72° corresponding to (1 1 1), (2 0 0), (2 2 0) and (3 1 1) planes, respectively. These peaks in the spectrum are specific to gold nanoparticles (Supplementary Fig. 2) revealing the face-centered cubic (FCC) crystal system, which matched well with the standard data file (JCPDS file no 04-0784). These results substantiate well with the gold nanoparticles synthesized using *Klebsiella pneumoniae* (Malarkodi et al., 2013). The absence of any other peak confirmed the high purity of synthesized gold nanoparticles. The peak broadening (Supplementary Fig. 2) is an indication of the smaller size of nanoparticles which is confirmed by calculating the crystallite size using the Scherrer's formula. The crystallite size was found to be ~14 nm for the peak based on the highest intensity (1 1 1) plane.

The gold nanoparticles were subjected to FESEM imaging to ascertain the morphological features. Low magnification image (Fig. 2a) shows the formation of spherical nanoparticles of size 8–30 nm. At higher magnification (Fig. 2b) the spherical gold nanoparticles were clearly observed. FESEM reveals that the spherical gold nanoparticles are embedded in biomatrix. Each spherical particle is made up of an aggregate of even
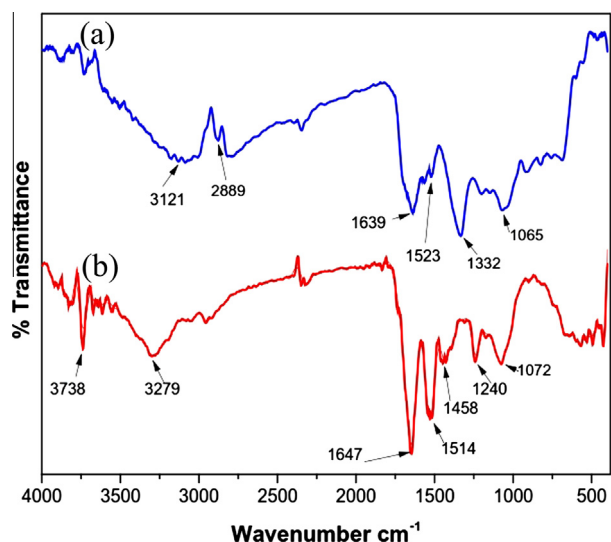
**Figure 5** FTIR spectra of (a) cell free extract and (b) gold nanoparticles.

smaller nanoparticles. TEM analysis confirmed the formation of almost spherical gold nanoparticles (Fig. 3a–c). The selected area electron diffraction (SAED) analysis revealed crystalline nature of nanoparticles exhibiting bright spots with lattice spacing corresponding to (111), (200), (220), and (311) planes of the FCC lattice of gold (Fig. 3d). The presence of bright spots in TEM images indicated the formation of extremely small nanocrystalline particles. The size of the particles was found to be in the range of 12–30 nm.

The particle size analysis using DLS revealed the presence of gold nanoparticles in the size range of 10–50 nm (Fig. 4).

Maximum nanoparticles lie between the size range of 10–20 nm with an average particle size of 13.5 ± 0.2 nm (vol. 73.21%). However, a few gold nanoparticles were found to be in the range of 20–50 nm with average particle size of 41.6 ± 9.7 nm (vol. 26.79%). This size of gold nanoparticles was larger than that observed in FESEM image (Fig. 3), which may be because DLS measures the hydrodynamic size (which is the size of the metallic core along with the coating material) (Adavallan and Krishnakumar, 2014). The presence of a few bigger size nanoparticles can be attributed to the agglomeration of gold nanoparticles. This agglomeration may be due to the lesser coating of the capping agent on the nuclei (which have been formed at the later stage of nucleation and growth).

The sizes obtained from XRD, DLS, FESEM and TEM were compared. It was observed that the average crystallite size obtained from DLS (13.5 nm) matches well with the crystallite size calculated from XRD (14 nm). Moreover, the particle size measured from FESEM images (8–30 nm) corroborates with that of TEM images (12–30 nm).

FTIR measurements of the CFE and CFE mediated gold nanoparticles can provide the information regarding the chemical change of the functional groups involved in the reduction of gold ions into gold nanoparticles (Fig. 5a and b). The IR spectrum of CFE showed distinct peaks at 3121 cm^{-1}, 2889 cm^{-1}, 1639 cm^{-1}, 1523 cm^{-1}, 1332 cm^{-1} and 1065 cm^{-1} (Fig. 5a). The peak at 3121 cm^{-1} may be attributed by N-H bending vibrations in amines. The peak at 2889 cm^{-1} could be due to C-H stretching vibrations in aldehydes. The peaks located at 1639 and 1523 cm^{-1} assigned to N-H bending vibrations in primary and secondary amines, respectively. The absorption band at 1332 cm^{-1} may be due to stretching vibrations of C-N aromatic functional group of proteins. The IR spectrum of CFE mediated gold nanoparticles showed peaks at 3738 cm^{-1}, 3279 cm^{-1}, 1647 cm^{-1}, 1514 cm^{-1}, 1458 cm^{-1} and 1240 cm^{-1} (Fig. 5b). The comparison of IR spectra of
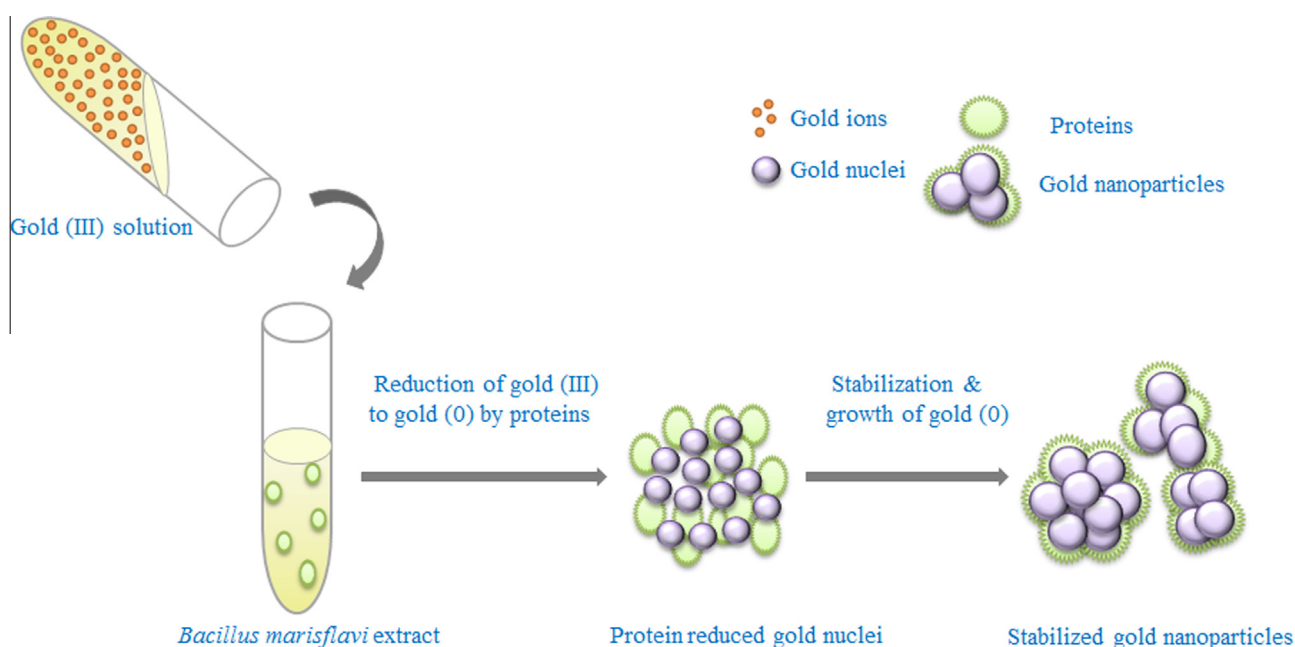

Figure 6 A plausible mechanism of the formation and stabilization of gold nanoparticles by the proteins present in the extract of *B. marisflavi*.

CFE with CFE mediated gold nanoparticles revealed that bands at 2889 and 1332 cm^{-1} in CFE were found to be masked in nanoparticles (Fig. 5b). This indicates that gold nanoparticles were in conjugation with aldehydes and functional groups of proteins. The slight shift in the peaks of functional groups to lower frequencies indicates that it might be involved in interactions with another group, thus confirming the capping mechanism (Kitching et al., 2015). In IR spectra, the shift in amino and carbonyl group of proteins present in CFE was observed (Fig. 5a). These results are in agreement with the previous report (Sarkar et al., 2012). The plausible mechanism of the formation of gold nanoparticles is shown in Fig. 6.

3.3. Catalytic activity of biosynthesized gold nanoparticles in the degradation of Congo red

The catalytic activity of biosynthesized gold nanoparticles in the presence of NaBH$_4$ was investigated by monitoring the

(a)

(b)
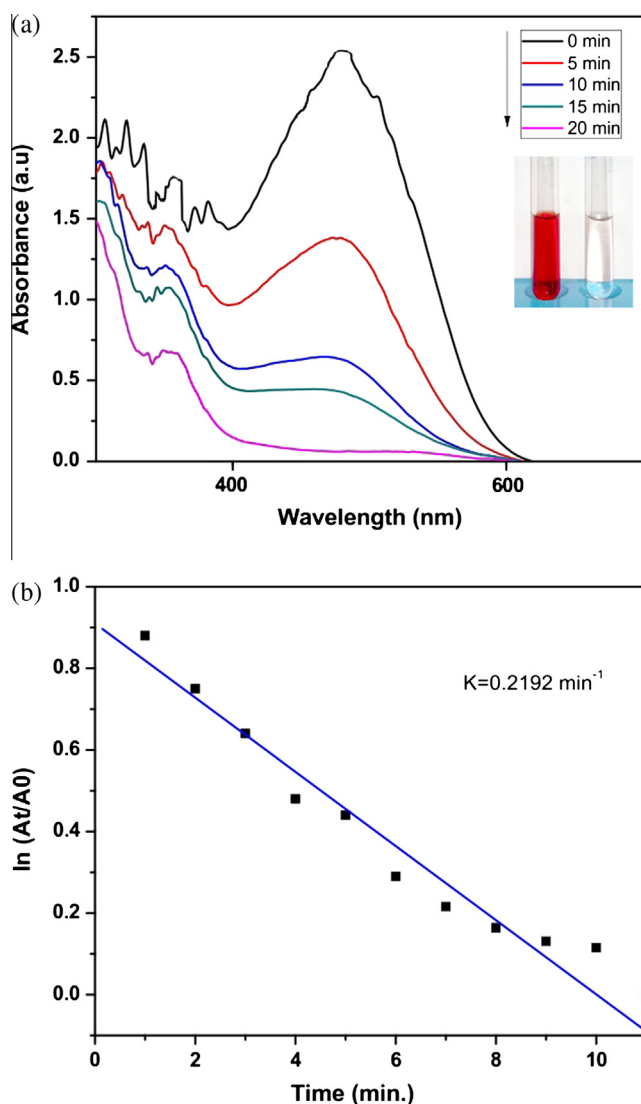
Figure 7 (a) UV-Visible absorbance spectra showing the degradation of Congo red using NaBH$_{4-}$ in the presence of gold nanoparticles (b) Plot of ln (A_t/A_0) versus time for the catalytic degradation of Congo red by biosynthesized gold nanoparticles.
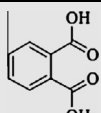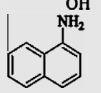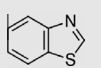
(a)

(b)
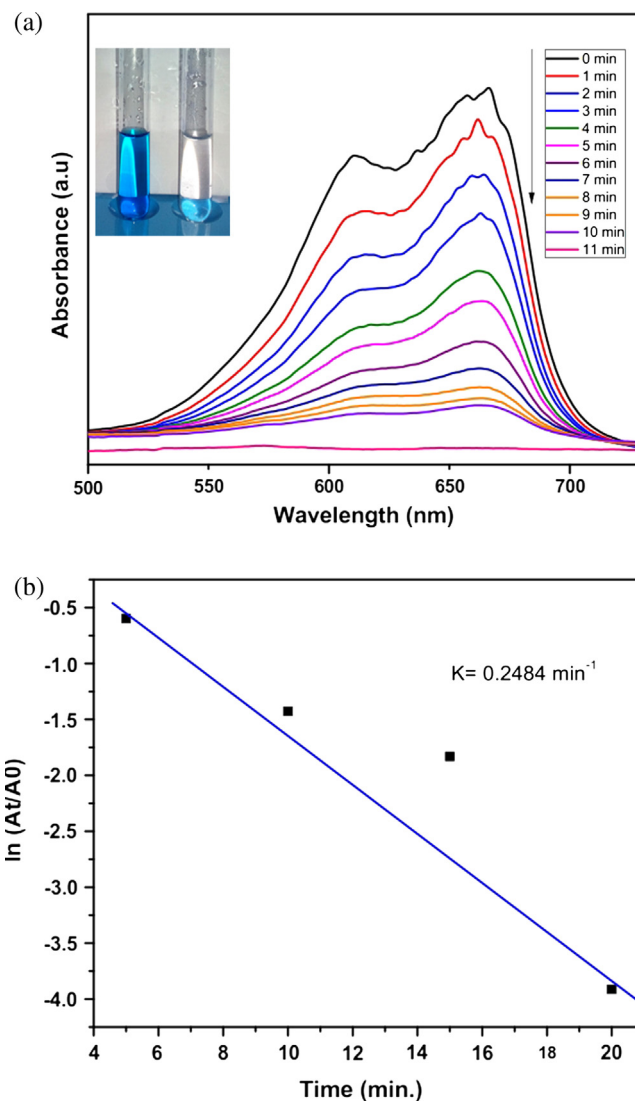
Figure 8 (a) UV-Visible absorbance spectra for the degradation of methylene blue using NaBH$_{4-}$ in the presence of gold nanoparticles (b) Plot of ln (A_t/A_0) versus time for the catalytic degradation of methylene blue by biosynthesized gold nanoparticles.

characteristic absorption peak at 486 nm in a UV-visible spectrophotometer (Fig. 7a). Interestingly, upon addition of gold nanoparticles into the mixture of Congo red and NaBH$_4$, gradual degradation of Congo red took place. The color of the solution changed from red to colorless within 20 min. During the reduction reaction, a gradual decrease in peak intensity (λ_{max}) at 486 nm was noticed. Within 20 min, the peak at 486 nm diminished, which indicates the degradation of Congo red. The SPR peak specific for gold nanoparticles was not seen in the UV-visible spectra of catalytic studies. This might be due to the presence of a very small quantity of nanoparticles with low concentration.

As the concentration of BH$_4^-$ was in much excess than Congo red, it was considered that the concentration remained constant throughout the reduction reaction. Hence, the reduction reaction was supposed to follow pseudo-first-order kinetics. A good linear correlation between ln (A_t/A_0) and time was

Table 1 Possible structures based on GC-MS data.

Dyes	Retention time	Possible structure of degraded dyes	m/z	References
Congo red	21.88		167	Natarajan et al. (2011)
	16.33		143	Natarajan et al. (2011)
Methylene blue	18.22		149	Lin et al. (2015)
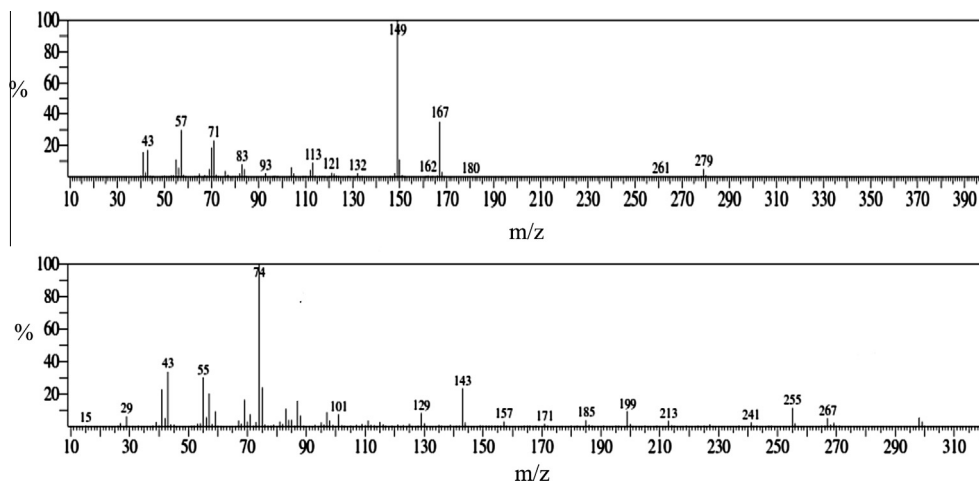
Figure 9 Mass spectra of degraded products of Congo red.

observed. From the plot of ln (A_t/A_0) vs time, the rate constant (K) value was calculated to be 0.2192 min^{-1} (Fig. 7b). The biosynthesized gold nanoparticles showed 98% Congo red degradation in the presence NaBH$_4$ within 20 min. In control, the Congo red degradation rate was found to be very slow with rate constant 0.0013 min^{-1} (Supplementary Fig. 3a and b). In the similar study carried out by Mata et al., (2015), degradation of Congo red took place within 40 and 60 min in the presence of 0.2 ml gold nanoparticles of size ~29 nm and ~16 nm, respectively.

3.4. Catalytic activity of biosynthesized gold nanoparticles in the degradation of methylene blue

Methylene blue is known to show maximum absorption band at 664 nm in an aqueous medium due to n-π* transition with shoulder peak at 614 nm (Cheval et al., 2012). The color of methylene blue is blue in an oxidized state and upon reduction, a colorless compound which is leuko methylene blue gets formed. When colloidal solution of gold nanoparticles was mixed with methylene blue and NaBH$_4$ solution, decolorization of methylene blue was observed. The completion of catalytic degradation of the dyes is considered when the absorbance value of methylene blue reached the baseline. The UV-visible spectroscopic study revealed the role of gold nanoparticles as a catalyst in the degradation of methylene blue by NaBH$_4$ (Fig. 8a). The absorption spectrum shows

the gradual decrease in a peak at 664 nm as a function of time. The degradation reaction kinetics followed the pseudo-first order reaction with a good linear correlation of ln (A_t/A_0) vs. time (min). From the plot of ln (A_t/A_0) vs. time, the rate constant (K) value was calculated to be 0.2484 min^{-1} (Fig. 8b). The biosynthesized gold nanoparticles showed 88% methylene blue degradation by NaBH$_4$ within 10 min, and complete catalytic degradation occurred within the next one minute. In the case of control, the time required for methylene blue degradation was far more with rate constant 0.0057 min^{-1} (Supplementary Fig. 4a and b).

Narayanan et al. (2015) demonstrated the reduction of methylene blue using intracellularly synthesized gold nanoparticles of size range few nanometers to 20 nm in the presence of NaBH$_4$ and the reduction process was reported to be completed within 23 min. However, Mata et al., (2015) observed the complete degradation of methylene blue occurred within 70 and 40 min by spherical gold nanoparticles of size ~29 nm and ~16 nm, respectively. Narayanan and Park (2014) also reported that the catalytic reduction of methylene blue using gold nanoparticles of average size ~32 nm in the presence of NaBH$_4$ required 18 min. In comparison with these reports, our biosynthesized gold nanoparticles assist faster degradation of methylene blue in the presence of NaBH$_4$ and hence can be used as superior nanocatalyst.

Gold nanoparticles help the electron relay from donor to the acceptor. The probable explanation of the catalytic activity
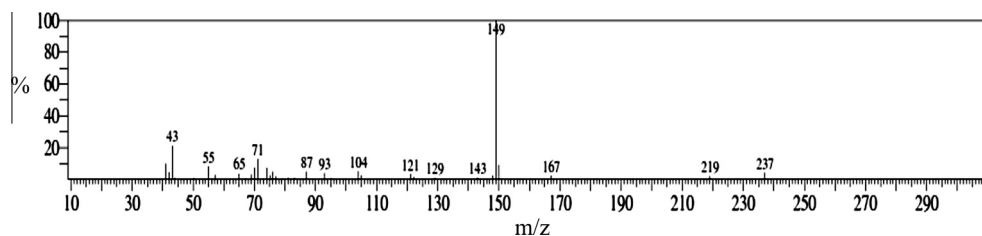
Figure 10   Mass spectra of degraded products of methylene blue.

of gold nanoparticles may be due to the fact that smaller size gold nanoparticles show greater surface area and facilitate the adsorption of dye and reducing agent BH_4. These gold nanoparticles act as donor as well as acceptor of electrons and help the electron relay (promotes the extent of reaction) in a redox reaction, hence transfer the surface hydride ions (donor) to the acceptor (dye/methylene blue/Congo red) (Mallick et al., 2006; Narayanan and Sakthivel, 2011; Wunder et al., 2011). Therefore, in the Congo red and methylene blue reduction reactions, our biosynthesized gold nanoparticles due to smaller particle size act as a potential catalyst by taking part in electron transfer process.

3.5. Gas chromatography-mass spectroscopy (GC-MS) analysis of degraded dyes

The analysis of degradation of Congo red and methylene blue using gold nanoparticles was carried out by GC-MS (Table 1). The GC-MS analysis revealed that the formation of intermediate metabolites upon breakdown of Congo red gives rise to signals at m/z = 143 and m/z = 167 (Fig. 9). These metabolites were identified as α naphthylamine and phthalic acid, respectively. These intermediates match with those shown in the proposed pathway of degradation of Congo red (Natarajan et al., 2011). The intermediate products formed after degradation of methylene blue showed signal at m/z = 149 and it was identified as 2- methyl benzothiazole (Fig. 10). This product formed can be correlated to the intermediate product formed in the studies of degradation of methylene blue (Lin et al., 2015). It is clear from the GC-MS results that the gold nanoparticles catalyzed the degradation of Congo red and methylene blue into low molecular weight compounds.

4. Conclusion

In this study eco-friendly synthesis of gold nanoparticles using an estuarine isolate, *Bacillus marisflavi* is reported for the first time. The biosynthesized gold nanoparticles were thoroughly characterized by UV- visible spectroscopy, XRD, FESEM, TEM and DLS which revealed spherical, face-centered cubic structures of gold nanoparticles having size ~14 nm. The catalytic study confirms the potential of biosynthesized gold nanoparticles in the degradation of Congo red and methylene blue. GC-MS analysis further confirmed degradation of Congo red into α naphthylamine and phthalic acid and methylene blue to 2-methyl benzothiazole.

Conflicts of interest

The authors declare no conflict of interest.

References

Adavallan, K., Krishnakumar, N., 2014. Mulberry leaf extract mediated synthesis of gold nanoparticles and its anti-bacterial activity against human pathogens. Adv. Nat. Sci. Nanosci. Nanotechnol. 5, 025018.

Baharara, J., Ramezani, T., Divsalar, A., Mousavi, M., Seyedarabi, A., 2016. Induction of apoptosis by green synthesized gold nanoparticles through activation of caspase-3 and 9 in human cervical cancer cells. Avicenna J. Med. Biotechnol. 8, 75.

Cheval, N., Gindy, N., Flowkes, C., Fahmi, A., 2012. Polyamide 66 microspheres metallised with in situ synthesised gold nanoparticles for a catalytic application. Nanoscale Res. Lett. 7, 1–9.

Cohen, M.R., Smetzer, J.L., 2016. Methylene blue is a monoamine oxidase inhibitor; severe harm and death associated with low-dose methotrexate; potentially dangerous mix-up between cancer drugs. Hosp. Pharm. 51, 110–114.

Elbeshehy, E.K., Elazzazy, A.M., Aggelis, G., 2015. Silver nanoparticles synthesis mediated by new isolates of *Bacillus* spp., nanoparticle characterization and their activity against Bean Yellow Mosaic Virus and human pathogens. Front. Microbiol. 6.

Fernández-Llamosas, H., Castro, L., Blázquez, M.L., Díaz, E., Carmona, M., 2016. Biosynthesis of selenium nanoparticles by *Azoarcus* sp. CIB. Microb. Cell Fact. 15, 1.

Gillman, P.K., 2006. Methylene blue implicated in potentially fatal serotonin toxicity. Anaesthesia 61, 1013–1014.

Hu, M., Chen, J., Li, Z.Y., Au, L., Hartland, G.V., Li, X., Marquez, M., Xia, Y., 2006. Gold nanostructures: engineering their plasmonic properties for biomedical applications. Chem. Soc. Rev. 35, 1084–1094.

Khan, R., Fulekar, M.H., 2016. Biosynthesis of titanium dioxide nanoparticles using *Bacillus amyloliquefaciens* culture and enhancement of its photocatalytic activity for the degradation of a sulfonated textile dye Reactive Red 31. J Colloid Interf. Sci. 475, 184–191.

Kitching, M., Ramani, M., Marsili, E., 2015. Fungal biosynthesis of gold nanoparticles: mechanism and scale up. Microb. Biotechnol. 8, 904–917.

Lin, J., Weng, X., Jin, X., Megharaj, M., Naidu, R., Chen, Z., 2015. Reactivity of iron-based nanoparticles by green synthesis under various atmospheres and their removal mechanism of methylene blue. RSC Adv. 5, 70874–70882.

Malarkodi, C., Rajeshkumar, S., Vanaja, M., Paulkumar, K., Gnanajobitha, G., Annadurai, G., 2013. Eco-friendly synthesis and characterization of gold nanoparticles using *Klebsiella pneumoniae*. J. Nanostruct. Chem. 3, 1–7.

Mallick, K., Witcomb, M., Scurrell, M., 2006. Silver nanoparticle catalysed redox reaction: an electron relay effect. Mater. Chem. Phys. 97, 283–287.

Mata, R., Bhaskaran, A., Sadras, S.R., 2015. Green-synthesized gold nanoparticles from *Plumeria alba* flower extract to augment catalytic degradation of organic dyes and inhibit bacterial growth. Particuology 24, 78–86.

Nadaf, N.Y., Kanase, S.S., 2015. Antibacterial activity of silver nanoparticles singly and in combination with third generation antibiotics against bacteria causing hospital acquired infections biosynthesized by isolated *Bacillus marisflavi* YCIS MN 5. Dig. J. Nanomater. Bios. 10, 1189–1199.

Narayanan, K.B., Park, H.H., 2014. Homogeneous catalytic activity of gold nanoparticles synthesized using turnip (*Brassica rapa* L.) leaf extract in the reductive degradation of cationic azo dye. Korean J. Chem. Eng. 32, 1273–1277.

Narayanan, K.B., Sakthivel, N., 2011. Heterogeneous catalytic reduction of anthropogenic pollutant, 4-nitrophenol by silver-bio-nanocomposite using *Cylindrocladium floridanum*. Bioresource Technol. 102, 10737–10740.

Narayanan, K.B., Park, H.H., Han, S.S., 2015. Synthesis and characterization of biomatrixed-gold nanoparticles by the mushroom *Flammulina velutipes* and its heterogeneous catalytic potential. Chemosphere 141, 169–175.

Natarajan, T.S., Natarajan, K., Bajaj, H.C., Tayade, R.J., 2011. Energy efficient UV-LED source and TiO_2 nanotube array-based reactor for photocatalytic application. Ind. Eng. Chem. Res. 50, 7753–7762.

Njoki, P.N., Lim, I.I.S., Mott, D., Park, H.Y., Khan, B., Mishra, S., Sujakumar, R., Luo, J., Zhong, C.J., 2007. Size correlation of optical and spectroscopic properties for gold nanoparticles. J. Phys. Chem. C 111, 14664–14669.

Philip, D., 2010. Rapid green synthesis of spherical gold nanoparticles using *Mangifera indica* leaf. Spectrochim. Acta A 77, 807–810.

Rai, M., Gade, A., Yadav, A., 2011. Biogenic nanoparticles: an introduction to what they are, how they are synthesized and their applications. In: Metal Nanoparticles in Microbiology. Springer, Berlin Heidelberg, pp. 1–14.

Saha, K., Agasti, S.S., Kim, C., Li, X., Rotello, V.M., 2012. Gold nanoparticles in chemical and biological sensing. Chem. Rev. 112, 2739–2779.

Sarkar, J., Ray, S., Chattopadhyay, D., Laskar, A., Acharya, K., 2012. Mycogenesis of gold nanoparticles using a phytopathogen *Alternaria alternata*. Bioprocess Biosyst. Eng. 35, 637–643.

Singh, P., Kim, Y.J., Zhang, D., Yang, D.C., 2016. Biological synthesis of nanoparticles from plants and microorganisms. Trends Biotechnol.

Srivastava, S.K., Constanti, M., 2012. Room temperature biogenic synthesis of multiple nanoparticles (Ag, Pd, Fe, Rh, Ni, Ru, Pt Co, and Li) by *Pseudomonas aeruginosa* SM1. J. Nanopart. Res. 14, 1–10.

Velusamy, P., Kumar, G.V., Jeyanthi, V., Das, J., Pachaiappan, R., 2016. Bio-inspired green nanoparticles: synthesis, mechanism, and antibacterial application. Toxicol. Res. 32, 95.

Versiani, A.F., Andrade, L.M., Martins, E.M., Scalzo, S., Geraldo, J.M., Chaves, C.R., Ferreira, D.C., Ladeira, M., Guatimosim, S., Ladeira, L.O., da Fonseca, F.G., 2016. Gold nanoparticles and their applications in biomedicine. Future Virol. 11, 293–309.

Wunder, S., Lu, Y., Albrecht, M., Ballauff, M., 2011. Catalytic activity of faceted gold nanoparticles studied by a model reaction: evidence for substrate-induced surface restructuring. Acs Catal. 1, 908–916.

Zhang, X.F., Shen, W., Gurunathan, S., 2016. Biologically synthesized gold nanoparticles ameliorate cold and heat stress-induced oxidative stress in *Escherichia coli*. Molecules 21, 731.